arXiv:1602.04488v2 [astro-ph.HE] 23 Feb 2016

Fermi-LAT Observations of the LIGO Event GW150914

M. Ackermann[1], M. Ajello[2], A. Albert[3], B. Anderson[4,5], M. Arimoto[6], W. B. Atwood[7], M. Axelsson[8,9], L. Baldini[10,3], J. Ballet[11], G. Barbiellini[12,13], M. G. Baring[14], D. Bastieri[15,16], J. Becerra Gonzalez[17,18], R. Bellazzini[19], E. Bissaldi[20], R. D. Blandford[3], E. D. Bloom[3], R. Bonino[21,22], E. Bottacini[3], T. J. Brandt[17], J. Bregeon[23], R. J. Britto[24], P. Bruel[25], R. Buehler[1], T. H. Burnett[26], S. Buson[17,27,28,29], G. A. Caliandro[3,30], R. A. Cameron[3], R. Caputo[7], M. Caragiulo[31,20], P. A. Caraveo[32], J. M. Casandjian[11], E. Cavazzuti[33], E. Charles[3], A. Chekhtman[34], J. Chiang[3], G. Chiaro[16], S. Ciprini[33,35], J. Cohen-Tanugi[23], L. R. Cominsky[36], B. Condon[37], F. Costanza[20], A. Cuoco[21,22], S. Cutini[33,38,35], F. D'Ammando[39,40], F. de Palma[20,41], R. Desiante[42,21], S. W. Digel[3], N. Di Lalla[19], M. Di Mauro[3], L. Di Venere[31,20], A. Domínguez[2], P. S. Drell[3], R. Dubois[3], D. Dumora[37], C. Favuzzi[31,20], S. J. Fegan[25], E. C. Ferrara[17], A. Franckowiak[3], Y. Fukazawa[43], S. Funk[44], P. Fusco[31,20], F. Gargano[20], D. Gasparrini[33,35], N. Gehrels[17], N. Giglietto[31,20], M. Giomi[1], P. Giommi[33], F. Giordano[31,20], M. Giroletti[39], T. Glanzman[3], G. Godfrey[3], G. A. Gomez-Vargas[45,46], J. Granot[47], D. Green[18,17], I. A. Grenier[11], M.-H. Grondin[37], J. E. Grove[48], L. Guillemot[49,50], S. Guiriec[17,51], D. Hadasch[52], A. K. Harding[17], E. Hays[17], J.W. Hewitt[53], A. B. Hill[54,3], D. Horan[25], T. Jogler[3], G. Jóhannesson[55], T. Kamae or Tuneyoshi Kamae[56], S. Kensei[43], D. Kocevski[17], M. Kuss[19], G. La Mura[16,52], S. Larsson[8,5], L. Latronico[21], M. Lemoine-Goumard[37], J. Li[57], L. Li[8,5], F. Longo[12,13], F. Loparco[31,20], M. N. Lovellette[48], P. Lubrano[35], G. M. Madejski[3], J. Magill[18], S. Maldera[21], A. Manfreda[19], M. Marelli[32], M. Mayer[1], M. N. Mazziotta[20], J. E. McEnery[17,18,58], M. Meyer[4,5], P. F. Michelson[3], N. Mirabal[17,51], T. Mizuno[59], A. A. Moiseev[28,18], M. E. Monzani[3], E. Moretti[60], A. Morselli[46], I. V. Moskalenko[3], S. Murgia[61], M. Negro[21,22], E. Nuss[23], T. Ohsugi[59], N. Omodei[3,62], M. Orienti[39], E. Orlando[3], J. F. Ormes[63], D. Paneque[60,3], J. S. Perkins[17], M. Pesce-Rollins[19,3], F. Piron[23], G. Pivato[19], T. A. Porter[3], J. L. Racusin[17,64], S. Rainò[31,20], R. Rando[15,16], S. Razzaque[24], A. Reimer[52,3], O. Reimer[52,3], T. Reposeur[37], S. Ritz[7], L. S. Rochester[3], R. W. Romani[3], P. M. Saz Parkinson[7,65], C. Sgrò[19], D. Simone[20], E. J. Siskind[66], D. A. Smith[37], F. Spada[19], G. Spandre[19], P. Spinelli[31,20], D. J. Suson[67], H. Tajima[68,3], J. G. Thayer[3], J. B. Thayer[3], D. J. Thompson[17], L. Tibaldo[69], D. F. Torres[57,70], E. Troja[17,18], Y. Uchiyama[71], T. M. Venters[17], G. Vianello[3,72], K. S. Wood[48], M. Wood[3], G. Zaharijas[73,74], S. Zhu[18], S. Zimmer[4,5]

[1]Deutsches Elektronen Synchrotron DESY, D-15738 Zeuthen, Germany

[2]Department of Physics and Astronomy, Clemson University, Kinard Lab of Physics, Clemson, SC 29634-0978, USA

[3]W. W. Hansen Experimental Physics Laboratory, Kavli Institute for Particle Astrophysics and Cosmology, Department of Physics and SLAC National Accelerator Laboratory, Stanford University, Stanford, CA 94305, USA

[4]Department of Physics, Stockholm University, AlbaNova, SE-106 91 Stockholm, Sweden

[5]The Oskar Klein Centre for Cosmoparticle Physics, AlbaNova, SE-106 91 Stockholm, Sweden

[6]Department of Physics, Tokyo Institute of Technology, Meguro City, Tokyo 152-8551, Japan

[7]Santa Cruz Institute for Particle Physics, Department of Physics and Department of Astronomy and Astrophysics, University of California at Santa Cruz, Santa Cruz, CA 95064, USA

[8]Department of Physics, KTH Royal Institute of Technology, AlbaNova, SE-106 91 Stockholm, Sweden

[9]Tokyo Metropolitan University, Department of Physics, Minami-osawa 1-1, Hachioji, Tokyo 192-0397, Japan

[10]Università di Pisa and Istituto Nazionale di Fisica Nucleare, Sezione di Pisa I-56127 Pisa, Italy

[11]Laboratoire AIM, CEA-IRFU/CNRS/Université Paris Diderot, Service d'Astrophysique, CEA Saclay, F-91191 Gif sur Yvette, France

[12]Istituto Nazionale di Fisica Nucleare, Sezione di Trieste, I-34127 Trieste, Italy

[13]Dipartimento di Fisica, Università di Trieste, I-34127 Trieste, Italy

[14]Rice University, Department of Physics and Astronomy, MS-108, P. O. Box 1892, Houston, TX 77251, USA

[15]Istituto Nazionale di Fisica Nucleare, Sezione di Padova, I-35131 Padova, Italy

[16]Dipartimento di Fisica e Astronomia "G. Galilei", Università di Padova, I-35131 Padova, Italy

[17]NASA Goddard Space Flight Center, Greenbelt, MD 20771, USA

[18]Department of Physics and Department of Astronomy, University of Maryland, College Park, MD 20742, USA

[19]Istituto Nazionale di Fisica Nucleare, Sezione di Pisa, I-56127 Pisa, Italy

[20]Istituto Nazionale di Fisica Nucleare, Sezione di Bari, I-70126 Bari, Italy

[21]Istituto Nazionale di Fisica Nucleare, Sezione di Torino, I-10125 Torino, Italy

[22]Dipartimento di Fisica Generale "Amadeo Avogadro" , Università degli Studi di Torino, I-10125 Torino, Italy

[23]Laboratoire Univers et Particules de Montpellier, Université Montpellier, CNRS/IN2P3, Montpellier, France

[24]Department of Physics, University of Johannesburg, PO Box 524, Auckland Park 2006, South Africa

[25]Laboratoire Leprince-Ringuet, École polytechnique, CNRS/IN2P3, Palaiseau, France

[26]Department of Physics, University of Washington, Seattle, WA 98195-1560, USA

[27]Department of Physics and Center for Space Sciences and Technology, University of Maryland Baltimore County, Baltimore, MD 21250, USA

[28]Center for Research and Exploration in Space Science and Technology (CRESST) and NASA Goddard Space Flight Center, Greenbelt, MD 20771, USA

[29]email: sara.buson@gmail.com

[30]Consorzio Interuniversitario per la Fisica Spaziale (CIFS), I-10133 Torino, Italy

[31]Dipartimento di Fisica “M. Merlin" dell’Università e del Politecnico di Bari, I-70126 Bari, Italy

[32]INAF-Istituto di Astrofisica Spaziale e Fisica Cosmica, I-20133 Milano, Italy

[33]Agenzia Spaziale Italiana (ASI) Science Data Center, I-00133 Roma, Italy

[34]College of Science, George Mason University, Fairfax, VA 22030, resident at Naval Research Laboratory, Washington, DC 20375, USA

[35]Istituto Nazionale di Fisica Nucleare, Sezione di Perugia, I-06123 Perugia, Italy

[36]Department of Physics and Astronomy, Sonoma State University, Rohnert Park, CA 94928-3609, USA

[37]Centre d’Études Nucléaires de Bordeaux Gradignan, IN2P3/CNRS, Université Bordeaux 1, BP120, F-33175 Gradignan Cedex, France

[38]INAF Osservatorio Astronomico di Roma, I-00040 Monte Porzio Catone (Roma), Italy

[39]INAF Istituto di Radioastronomia, I-40129 Bologna, Italy

[40]Dipartimento di Astronomia, Università di Bologna, I-40127 Bologna, Italy

[41]Università Telematica Pegaso, Piazza Trieste e Trento, 48, I-80132 Napoli, Italy

[42]Università di Udine, I-33100 Udine, Italy

[43]Department of Physical Sciences, Hiroshima University, Higashi-Hiroshima, Hiroshima 739-8526, Japan

[44]Erlangen Centre for Astroparticle Physics, D-91058 Erlangen, Germany

[45]Instituto de Astrofísica, Facultad de Física, Pontificia Universidad Católica de Chile, Casilla 306, Santiago 22, Chile

[46]Istituto Nazionale di Fisica Nucleare, Sezione di Roma “Tor Vergata", I-00133 Roma, Italy

[47]Department of Natural Sciences, Open University of Israel, 1 University Road, POB 808, Ra’anana 43537, Israel

[48]Space Science Division, Naval Research Laboratory, Washington, DC 20375-5352, USA

[49]Laboratoire de Physique et Chimie de l’Environnement et de l’Espace – Université d’Orléans / CNRS, F-45071 Orléans Cedex 02, France

[50]Station de radioastronomie de Nançay, Observatoire de Paris, CNRS/INSU, F-18330 Nançay, France

[51]NASA Postdoctoral Program Fellow, USA

[52]Institut für Astro- und Teilchenphysik and Institut für Theoretische Physik, Leopold-Franzens-Universität Innsbruck, A-6020 Innsbruck, Austria

[53]University of North Florida, Department of Physics, 1 UNF Drive, Jacksonville, FL 32224 , USA

[54]School of Physics and Astronomy, University of Southampton, Highfield, Southampton, SO17 1BJ, UK

[55]Science Institute, University of Iceland, IS-107 Reykjavik, Iceland

[56]Department of Physics, Graduate School of Science, University of Tokyo, 7-3-1 Hongo, Bunkyo-ku, Tokyo 113-0033, Japan

[57]Institute of Space Sciences (IEEC-CSIC), Campus UAB, E-08193 Barcelona, Spain

[58]email: Julie.E.McEnery@nasa.gov

[59]Hiroshima Astrophysical Science Center, Hiroshima University, Higashi-Hiroshima, Hiroshima 739-8526, Japan

[60]Max-Planck-Institut für Physik, D-80805 München, Germany

ABSTRACT

The *Fermi* Large Area Telescope (LAT) has an instantaneous field of view covering $\sim 1/5$ of the sky and completes a survey of the entire sky in high-energy gamma rays every 3 hours. It enables searches for transient phenomena over timescales from milliseconds to years. Among these phenomena could be electromagnetic counterparts to gravitational wave sources. In this paper, we present a detailed study of the LAT observations relevant to Laser Interferometer Gravitational-wave Observatory (LIGO) event GW150914 (Abbott et al. 2016), which is the first direct detection of gravitational waves and has been interpreted as due to the coalescence of two stellar-mass black holes.The localization region for GW150914 was outside the LAT field of view at the time of the gravitational-wave signal. However, as part of routine survey observations, the LAT observed the entire LIGO localization region within ~ 70 minutes of the trigger, and thus enabled a comprehensive search for a γ-ray counterpart to GW150914. The study of the LAT data presented here did not find any potential counterparts to GW150914, but it did provide limits on the presence of a transient counterpart above 100 MeV on timescales of hours to days over the entire GW150914 localization region.

Subject headings: gravitational waves, gamma rays: general, methods: observational

[61]Center for Cosmology, Physics and Astronomy Department, University of California, Irvine, CA 92697-2575, USA

[62]email: nicola.omodei@stanford.edu

[63]Department of Physics and Astronomy, University of Denver, Denver, CO 80208, USA

[64]email: judith.racusin@nasa.gov

[65]Department of Physics, The University of Hong Kong, Pokfulam Road, Hong Kong, China

[66]NYCB Real-Time Computing Inc., Lattingtown, NY 11560-1025, USA

[67]Department of Chemistry and Physics, Purdue University Calumet, Hammond, IN 46323-2094, USA

[68]Solar-Terrestrial Environment Laboratory, Nagoya University, Nagoya 464-8601, Japan

[69]Max-Planck-Institut für Kernphysik, D-69029 Heidelberg, Germany

[70]Institució Catalana de Recerca i Estudis Avançats (ICREA), Barcelona, Spain

[71]Department of Physics, 3-34-1 Nishi-Ikebukuro, Toshima-ku, Tokyo 171-8501, Japan

[72]email: giacomov@slac.stanford.edu

[73]Istituto Nazionale di Fisica Nucleare, Sezione di Trieste, and Università di Trieste, I-34127 Trieste, Italy

[74]Laboratory for Astroparticle Physics, University of Nova Gorica, Vipavska 13, SI-5000 Nova Gorica, Slovenia

1. Introduction

The ∼2.4 sr field of view (FoV) and broad energy coverage from 20 MeV to >300 GeV of the Large Area Telescope (LAT, Atwood et al. 2009) on the *Fermi Gamma-ray Space Telescope* mission make it a powerful instrument to monitor the sky for high-energy transients. As the LAT surveys the entire sky every 3 hours, it is sensitive to transient emission from a variety of sources, including stellar-mass compact objects (Neutron Stars – NS, and Black Holes – BH) over timescales from milliseconds to years, including those predicted to be associated with gravitational waves (GWs). Current GW detectors are sensitive to signals from the merging of compact objects. Some of these mergers, like the putative progenitors of short Gamma-Ray Bursts (sGRBs, Paczynski 1986; Eichler et al. 1989; Narayan et al. 1992; Rezzolla et al. 2011; Metzger & Berger 2012), emit both a short-lived γ-ray signal ($\lesssim 2$ s) immediately after the merger ("prompt" emission), and a long-lived and broadband "afterglow" signal lasting minutes to hours. If the GRB happens to be in the FoV at the time of the trigger, the LAT can detect the short-lived prompt emission phase. If the GRB is outside the FoV, because of its survey capability the LAT can still detect the GRB by measuring its temporally-extended afterglow emission as soon as it enters the FoV. The LAT has detected high-energy γ-ray emission from >130 GRBs to-date (Vianello et al. 2016), including ∼10 sGRBs. Given the uncertainty in theoretical predictions for counterparts to GW sources and the demonstrated emission of high-energy γ-rays from systems containing compact objects, searching the LAT data for γ-ray counterparts to GW events.

The era of gravitational wave astronomy has begun with the first science run ('O1') of the recently upgraded LIGO (Abramovici et al. 1992; Abbott et al. 2009) from 2015 September to 2016 January. The Virgo Observatory (Caron et al. 1999; Acernese et al. 2009) will soon be added to the network for the second science run in late 2016. The GW frequency range that LIGO and Virgo are sensitive to is expected to be dominated by mergers of compact stellar-mass objects that are most likely remnants of stellar evolution: two neutron stars (NS-NS), two black holes (BH-BH), or a NS and a BH. The sensitivity and horizon distance of the GW network to these mergers scales with the masses of the systems; therefore the accessible volume of the Universe for NS mergers is significantly smaller than that of BH mergers. When those mergers include at least one NS, an electromagnetic counterpart is predicted to accompany the merger signal in the form of a sGRB. The electromagnetic outcome of a BH-BH merger is less well understood. Finding the counterpart of a GW event is important for understanding the nature of the source. It also has an additional yet less-evident benefit: it improves significantly the accuracy with which all parameters (distance, mass, spin, inclination, etc.) can be estimated. This is obtained by better constraining the localization of the event, which is normally poorly estimated using only the GW signal (Sathyaprakash & Schutz 2009). *Fermi*-LAT can localize a transient source with sub-degree accuracy, a very big improvement with respect to a typical localization region from a GW detector, which will typically cover hundreds of square degrees.

On 2015 September 14 at 09:50:45 UTC the LIGO Hanford and Livingston installations detected a coincident signal, within 10 ms, from GW150914, a high-significance trigger in the engineering run just prior to the start of O1. The trigger was determined to be consistent with a waveform predicted by General Relativity from the inspiral and merger of a stellar-mass binary BH system, with constituent BHs of masses around 29 $M_\odot$ and 36 $M_\odot$ (Abbott et al. 2016). The GW luminosity expected theoretically for a massive

BH-BH merger leads to an estimate of around 400 Mpc (i.e., z$\sim$ 0.09, Abbott et al. 2016) for the distance of the source. This observation provides evidence for the existence of isolated and binary stellar-mass black holes, and the first observation of such a system merging. Two days later, on 2015 September 16, LIGO notified the electromagnetic (EM) partner observatories operating within a Memorandum of Understanding (MOU). The EM partner observatories executed follow-up programs (LIGO Collaboration et al. 2016) to search for a counterpart within the 750 deg^2 localization region ($\sim$ 90% confidence), which was later refined to 601 deg^2 (LIGO Collaboration et al. 2016). *Fermi* was operating in normal survey mode at the time of the trigger. Hence, the LAT autonomously observed the entire LIGO localization region within $\sim$ 70 minutes of the GW trigger, independently of any notification from LIGO, in the high-energy γ-ray band. The LAT Collaboration reported a preliminary search throughout the LIGO localization area that did not reveal any new γ-ray sources (Omodei et al. 2015). The results of a search of the data of the other instrument on board *Fermi*, the Gamma-Ray Burst Monitor (GBM, Meegan et al. 2009) and the evidence for a weak counterpart are discussed separately in Connaughton et al. (2016).

In this paper, we describe LAT observations of the localization area of GW150914 around the time of the trigger, including a dedicated search for an EM γ-ray counterpart. No candidate counterparts were found. We describe the details of the data analysis in §2, discuss the implications of the counterpart search and prospects for future GW triggers in §3, and conclude in §4.

2. Data analysis

We performed two complementary sets of searches for transient high-energy γ-ray emission: automated searches (§2.1) that are performed routinely on all LAT data, and targeted searches in the LIGO localization region (§2.2) on short and long time baselines that exploit the full sensitivity of the standard LAT analysis chain. In Appendix A, and B we provide more details on the various analysis steps.

2.1. Automated Searches

Since the launch of *Fermi* in 2008, automated on-board and on-ground analyses of GBM and LAT data have been in place to search for new transients at various time- and energy-scales. As our understanding of the instruments, data, and the variable and transient γ-ray sky has improved, so have our automated analyses. Three LAT pipelines were relevant to the counterpart search for GW150914:

- The Burst Advocate (BA) Tool and LAT Transient Factory (LTF) are automated pipelines that search for excess emission in the LAT data at the positions of triggers from GBM, *Swift*, INTEGRAL and MAXI at the time of the trigger and intervals in the hours afterwards. As there were no on-board triggers by any of these instruments coincident with GW150914, the BA Tool and LTF were not initiated. However, in the event of a LAT on-board trigger or a trigger from these observatories coincident with a GW trigger, the pipelines would perform an automated search once the LAT data

were available on the ground ($\sim$ 8 hours after trigger), with results monitored by on-shift personnel.

- Automated Science Processing (ASP; Chiang 2012) is the standard LAT search for transient or flaring sources on 6-hour, 24-hour, and 7-day timescales. The ASP pipeline performs a detection step via a blind search for sources on all-sky counts maps constructed from the event data acquired at each timescale; then, a standard likelihood analysis is run on those data using a source model that includes the candidate sources found in the detection step as well as the already known sources that have been designated for regular monitoring. LAT Flare Advocates (a.k.a. Gamma-ray Sky Watchers) offer a prompt human verification service to the automatic pipelines and review the results daily, providing an internal report to the LAT Collaboration. Relevant information on monitored, flaring and transient sources is released to the astrophysical community using the LAT multiwavelength mailing-list[1], Astronomer's Telegrams[2] and Gamma-ray Coordinates Network notices[3]. Weekly summary digests are made available through the *Fermi* Sky Blog[4]. The LAT Flare Advocate service has been very effective in identifying potential candidates for quick follow-up and coordinated observations at other wavelengths (Ciprini et al. 2013). ASP discovers an average of 8 previously unknown γ-ray transients per year, and has also detected bright GRB afterglows (e.g., GRB 130427A, Ackermann et al. 2014).

- *Fermi* All-sky Variability Analysis (FAVA) is a photometric technique that searches for new transients and variable sources on 7-day timescales (Ackermann et al. 2013b). This method compares the number of detected γ rays with the average number of expected γ rays based on the observed long-term average in a given region of the sky. In this way, FAVA provides a computationally inexpensive blind search of flux variations over the entire sky that is independent of both an assumed spectral shape of the flaring source and any model for the diffuse γ-ray background. The FAVA pipeline detects an average of 16 flares per week; about 10% of these are not associated with γ-ray catalog sources (e.g., Kocevski et al. 2014). Seven-day FAVA lightcurves for any position on the sky are publicly available at the FAVA Data Portal[5] hosted at NASA's *Fermi* Science Support Center (FSSC).

During the 6-hour interval[6] containing the LIGO trigger GW150914, ASP detected ($>3\sigma$) twelve known γ-ray sources and three low-significance ($>1\sigma$) unidentified transients, none consistent with the LIGO event localization. None of the LAT pipelines found a possible counterpart to GW150914.

[1]To sign up for the LAT multiwavelength list visit http://fermi.gsfc.nasa.gov/ssc/library/newsletter/

[2]https://www-glast.stanford.edu/cgi-bin/pub_rapid

[3]http://gcn.gsfc.nasa.gov/fermi_lat_mon_trans.html

[4]http://fermisky.blogspot.com

[5]http://fermi.gsfc.nasa.gov/ssc/data/access/lat/FAVA/

[6]The ASP 6-hour interval containing the LIGO trigger time includes LAT data between 2015 September 14, 06:11:33–12:00:00 UTC.

2.2. Search in the LIGO localization region

The LIGO Scientific Collaboration reported results from a Bayesian parameter estimation analysis of GW150914 under the assumption that the signal arises from a compact binary coalescence (CBC) using the latest offline calibration of the GW strain data. The most accurate localization map for this event (`LALInference`) is based on a Bayesian Markov-Chain Monte Carlo and nested sampling to forward model the full GW signal including spin precession and regression of systematic calibration errors. The localization probability is primarily in the southern portion of the annulus determined by the arrival time difference between LIGO Hanford and LIGO Livingston of ~ 7 ms.

Given the uncertainty on EM signals from the merging of two BHs, we searched different time windows by carrying out two customized analyses of the LAT data. Both analyses are based on the standard maximum likelihood analysis technique used for LAT data, and summarized in Appendix A. In all our searches we included in the likelihood model all sources (point-like and extended) from the LAT source catalog (3FGL, Acero et al. 2015), as well as the Galactic and isotropic diffuse templates provided by the *Fermi*-LAT collaboration[7]. We used the Pass 8 `P8_TRANSIENTR010E_V6` event class and the corresponding instrument response functions. These searches are described in the following sections.

2.2.1. Short-baseline search

This search focuses on the hours immediately after the GW trigger t_{GW} (2015 September 14, 09:50:45 UTC). The LAT can detect long and short GRB afterglows up to thousands of seconds after the end of the prompt emission (De Pasquale et al. 2010; Ackermann et al. 2013c; Vianello et al. 2015). Thus a search in this time window is the most likely to find a counterpart to GW150914 if it is similar to a sGRB. *Fermi* was in normal survey mode operations around t_{GW}, rocked 50° North from the orbital plane. We consider a point in the sky observable by LAT if it is within the 65° radius FoV and has an angle with respect to the local zenith smaller than 100°. The latter requirement is used to exclude contamination from γ-ray emission from the Earth's atmosphere. The *coverage* is the integral of the probability densities of all points in the LIGO localization probability map observable by LAT at a given time, and it is shown in Fig. 1 as a function of time. While the coverage was between 50% and 90% in the hours before the trigger (dashed line), at t_{GW} the LAT was unfortunately viewing the opposite side of the sky from the LIGO localization region. The coverage was zero until $\sim t_{GW}+4200$. The time interval $t_{GW}+4442$–4867 s (T_1) had coverage >90%, while during $t_{GW}+4867$–10000 s coverage varied between 50 and 98%, decreasing back to zero at around $t_{GW}+10$ ks. We searched for a transient source in the time interval having more than 90% coverage (T_1), and we did not find any significant excess.

We then derived upper limits for the γ-ray flux of GW150914. Since the sensitivity of the LAT depends

[7] http://fermi.gsfc.nasa.gov/ssc/data/access/lat/BackgroundModels.html

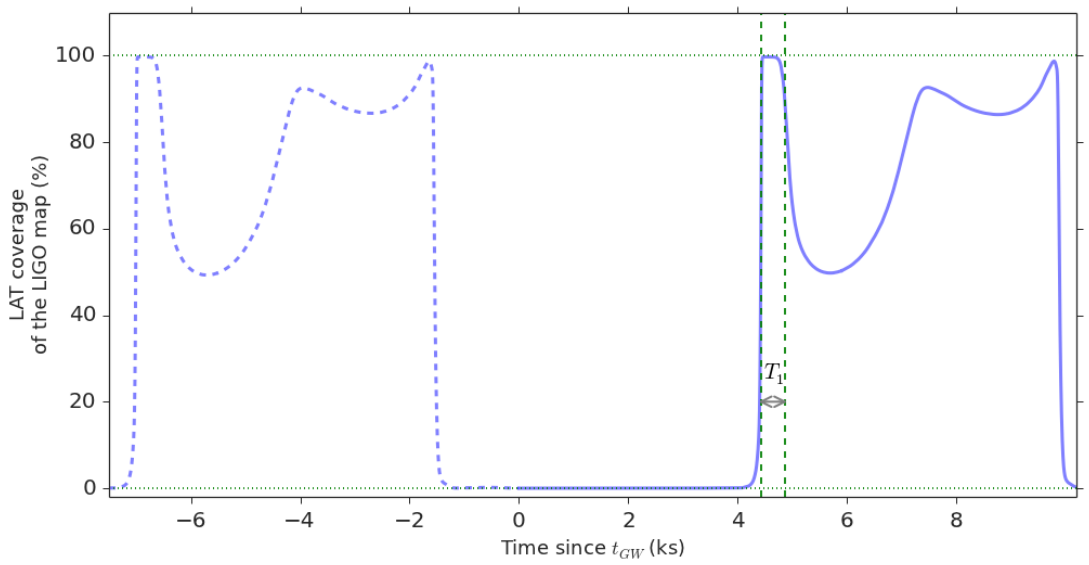


Fig. 1.— *Fermi*-LAT coverage (see text) of the LIGO localization map, as a function of time, before t_{gw} (dashed curve) and after t_{gw} (solid curve). The green dashed vertical lines denote the boundary of the interval T_1 used in the analysis (see text for details), while the horizontal dotted lines mark respectively 0% and 100% coverage.

strongly on the angle from the source to the boresight of the instrument, the continuous variation of the LAT viewing direction in survey mode makes any flux limit for a particular source position time-dependent. Flux limits are also sensitive to astrophysical backgrounds, particularly in the Galactic plane, so that positions along the LIGO arc will have different flux limits, even for the same observing conditions. These effects mean that flux limits vary according to both time of observation and position in the localization region. We show a map of the derived upper limits (95% confidence level) for the γ-ray flux of GW150914 in the band 100 MeV − 1 GeV in the left-hand panel of Fig. 2, and a histogram of the upper limits in the right-hand panel, both for interval T_1. Assuming a power-law spectrum for the source with a photon index of $\alpha = -2$, which is typical for GRB afterglows at LAT energies, the upper limits we find have a median of 1.7×10^{-9} erg cm^{-2}s^{-1}, and 5% and 95% percentiles of 0.9×10^{-9} and 3.7×10^{-9} erg cm^{-2}s^{-1}, respectively. These upper limits are only weakly dependent on the choice of α as shown in the right-hand panel of Fig. 2. We now describe the upper limits analysis in more detail.

We considered all γ-rays with reconstructed energies between 100 MeV and 100 GeV. We then considered the `LALInference` probability map provided by LIGO, which is a `HEALPix` map with `NSIDE = 512` (Górski et al. 2005), corresponding to a typical pixel size of $\sim 0.^{\circ}11$. The point-spread function (PSF) of the LAT has a 68% containment radius at 1 GeV of $\sim 1^{\circ}$. To save computation time, we resampled

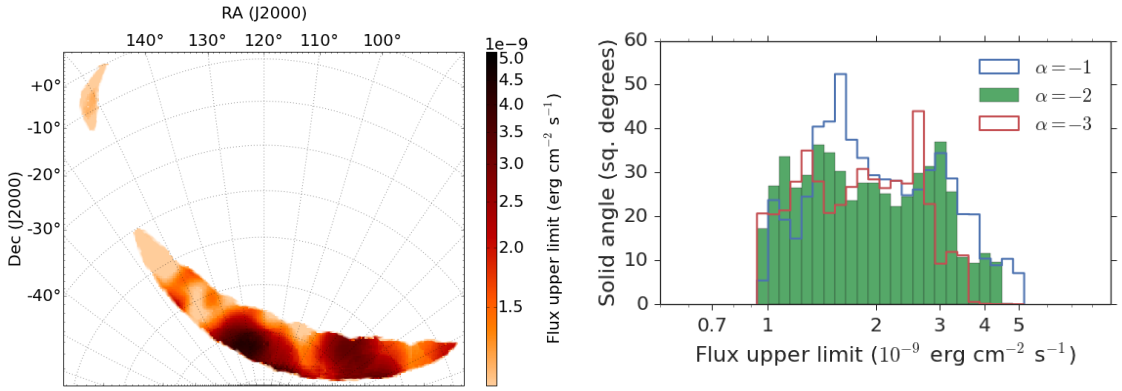


Fig. 2.— Flux upper limits (95% c.l.) in the energy range 100 MeV–1 GeV for GW150914 during the interval T_1 (4442–4867 s from t_{GW}). Left panel: upper limits map covering the 90% region of the LIGO probability map. Right panel: histogram of the upper limits in the map. We assumed a power-law spectrum for the source, with a photon index α of −2 (typical of afterglows of GRBs, green histogram), −1 (blue histogram) and −3 (red histogram). While the distributions are slightly different for the three cases, the ranges spanned by the upper limits are largely independent of the photon index.

the map to `NSIDE = 256`, which corresponds to a typical pixel size of ∼0.°2. We considered the 11463 pixels in the resampled map contained within the 90% containment region provided by LIGO. Let us denote $\vec{v_i}$ the direction of the center of the i-th pixel. For each i-th pixel we performed an independent likelihood analysis (see Appendix 2.1), considering a Region Of Interest (ROI) of 8° centered in $\vec{v_i}$ and testing for a new source at the position $\vec{v_i}$. For each likelihood analysis we required the zenith angle of the events to be no more than 100°. We did not find any new source with a test statistic (TS) above our adopted threshold of 25, corresponding to $\sim 5\sigma$ (pre-trials). We then computed the 95% confidence level upper limit for the flux of a source at each $\vec{v_i}$. In order to obtain upper limits reasonably independent of the photon index α adopted in the analysis we need to choose an energy range small enough. We have chosen the range 100 MeV–1 GeV for the upper limits, which provides the largest photon statistic and the maximum sensitivity for sources similar to GRBs. The right-hand panel of Figure 2 shows that our measurement is indeed largely independent of the choice of α.

Connaughton et al. (2016) reported the weak transient γ-ray source GW150914-GBM lasting $\sim$ 1 s, 0.4 s after the LIGO trigger on GW150914. GW150914-GBM is consistent with being due to a low-fluence sGRB at an unfavorable viewing geometry to the GBM detectors, although this is not expected from a BH-BH merger. Assuming the two signals have a common origin, the combined LIGO and GBM observations reduce the 90% confidence region from 601 deg^2 to 199 deg^2. Within the combined LIGO/GBM localization, and in the time interval T_1, the most significant excess in LAT data has TS = 18. We estimate for this excess a p-value of $\sim$ 0.05, taking into account the number of trials of our analysis, which corresponds to a significance that is well below our threshold of 5σ. The excess has a spectrum well modeled with a power

law with a soft photon index $\alpha = -3.2 \pm 0.8$, and it is located close the limb of the Earth (which has indeed a soft spectrum). Therefore we consider this excess in the LAT data very likely to be either a statistical fluctuation or due to Earth limb contamination, and therefore unrelated to GW150914 or GW150914-GBM.

2.2.2. Long-baseline search

In this second search we considered data gathered during a 2-month interval centered on t_{GW}. In order to increase the number of γ-rays we included all photons with energies between 60 MeV and 100 GeV. Since the PSF at 60 MeV is broad, we applied a zenith cut of 95° to further limit Earth limb contamination. We looked both for a long-duration signal of the order of one day, as well as for a short-duration signal but not necessarily in strict temporal coincidence with the LIGO trigger. To this end, we covered the entire 90% probability region provided by LIGO with a set of nine partially overlapping ROIs, each with a radius of 10°. Figure 3 shows the locations of these ROIs and the confidence contours obtained from the `LALInference` probability map. They are overlaid on a sky map of the γ-rays detected by the LAT over the interval t_{GW} to $t_{GW} + 10000$ s. In Table 1 we provide the location of the center of each ROI, listing all the LAT sources from the 3FGL catalog (Acero et al. 2015) within each ROI, along with their associations and their classes, using the same notation as the 3FGL catalog.

For the first analysis of the second search we divided the data in 10 ks time bins. For each time bin and for each ROI we calculated a TS map (see Appendix B) and determined the location of the grid position with the maximum TS (TS_{max}). We considered the position of TS_{max} as the location of a possible counterpart, and we ran an unbinned likelihood analysis adding a point source at the position of TS_{max}. This gave a value of TS_{src} (which is normally similar to TS_{max}). In these maps derived from low-statistics data single high-energy γ-rays can cause a high value of TS_{max}. To reduce the number of false positives from random coincidences, we required that the number of photons N_γ that have a probability larger than 0.9 to be associated with the candidate counterpart to be greater than 2. No excesses met this requirement. In Appendix B we present the TS maps for the 9 ROIs for the time interval 0–10 ks since t_{GW}. We repeated the same analysis considering time bins of 1 day, and again did not find any significant excess.

We also considered the possibility of excesses over shorter timescales (<1 h), similar to the typical duration of high-energy emission from GRBs (Ackermann et al. 2013c; Vianello et al. 2015), but not in temporal coincidence with the GW trigger and hence not covered by the "short-baseline" search described in §2.2.1. We calculated the entry and exit times for each ROI in the FoV of the LAT (a "FoV passage"), requiring that the distance between the LAT boresight and the center of the ROI be <60°. In standard survey mode, the duration of a FoV passage varies from a few hundred seconds to nearly one hour. Since we do not know if an EM signal would be in temporal coincidence with the GW signal, we searched for possible excesses in every passage, corresponding to a total of 6615 passages for each ROI. We did not detect any significant excess in any of the passages before or after t_{GW} for any ROI.

Figure 4 displays the four TS maps with the highest TS_{src} and $N_\gamma > 2$. The first map ($TS_{src} = 21$) is from the first ROI and corresponds to the passage from 22:15:53 to 22:20:30 UTC on 2015 October 10

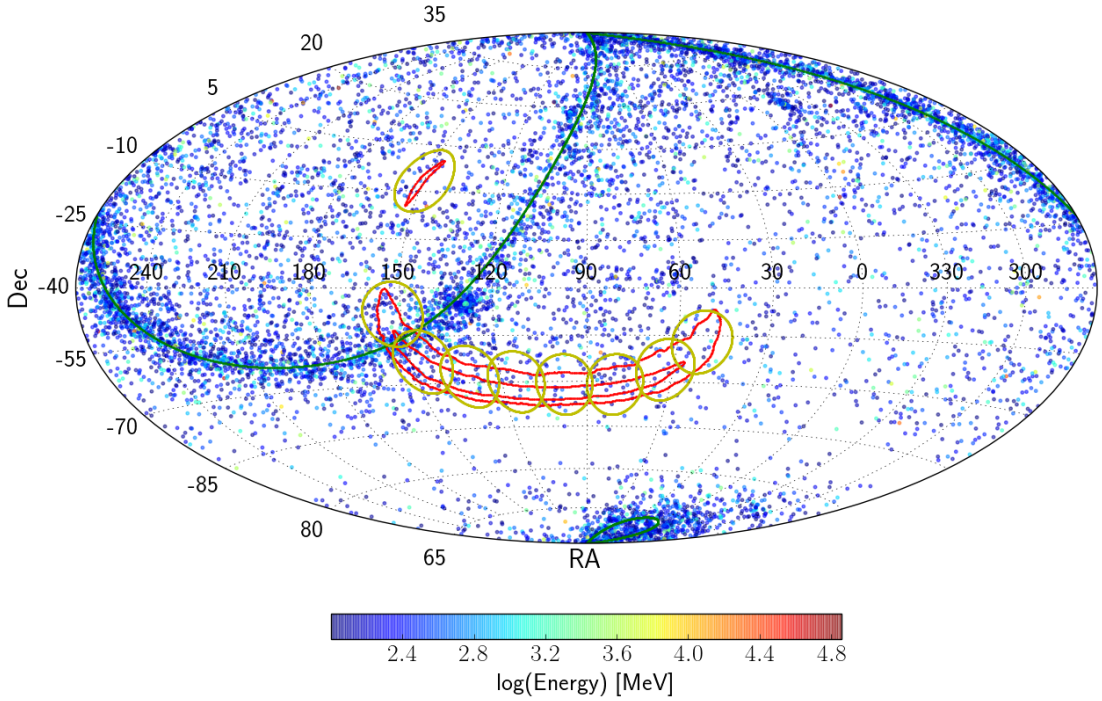


Fig. 3.— LAT-detected γ-rays in celestial coordinates (J2000) in the interval from t_{GW} to t_{GW}+10000s, and in the energy range 60 MeV–100 GeV. The dots are colored according to energies of the γ rays as indicated in the color bar. The highest-energy photon recorded in this time interval has an energy of $\sim$ 60 GeV, corresponding to the maximum of the color bar. The 90% and 50% contour levels from `LALInference` are overlaid on the image, in red. The map is in `Hammer-Aitoff` projection and is centered at R.A., Dec= 90°, –40°. The Galactic plane is highlighted in green. The nine LAT ROIs where we perform the searches described in §2.2.2 are shown as yellow circles.

(17.5 days after the trigger time t_{GW}). The second map is from the third ROI in the passage from 17:47:41 to 17:56:41 UTC on 2015 August 21 (20.7 days before t_{GW}), and has also a $TS_{src} = 21$. The third map ($TS_{src} = 22$) is from the seventh ROI in the interval from 21:35:48 to 21:50:01 UTC on 2015 August 20 (24.5 days before t_{GW}). Finally, the last map is from the eighth ROI, during 12:59:40 to 13:39:41 UTC on 2015 September 17 (3.1 days after the trigger LIGO trigger time t_{GW}) has the highest value of TS with $TS_{src} = 23$. The peak TS values correspond to low-energy γ rays in random coincidence with high-energy γ rays, and the highest values obtained in this analysis should not be considered indicative of a possible EM counterpart. Moreover, the above search involves a large number of trials. To estimate their impact on the

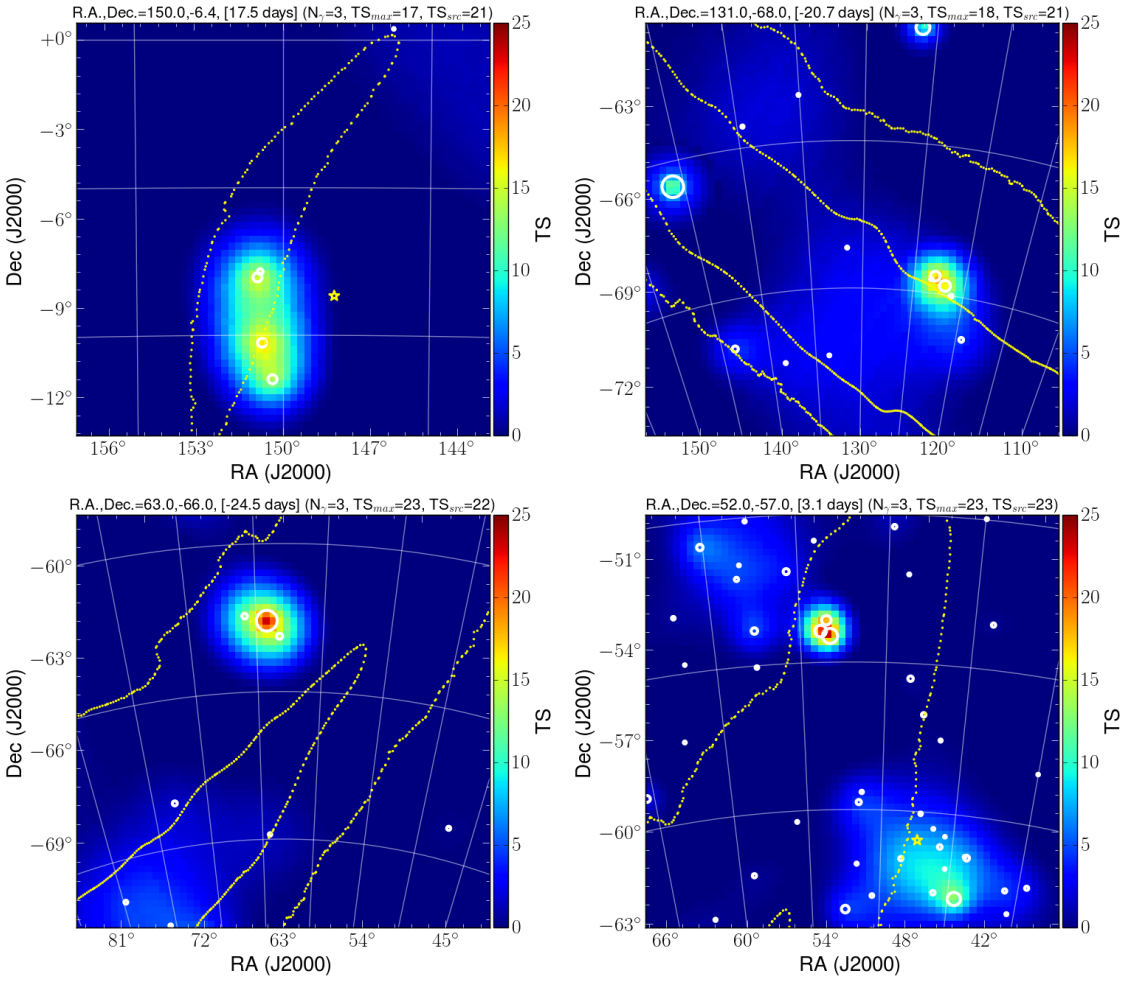


Fig. 4.— TS maps of the most significant excesses detected over one-orbit timescales ($\sim$ minutes) within 30 days before or after the LIGO trigger. Yellow stars are sources from the 3FGL catalog, and circles are individual LAT γ rays with their size proportional to the reconstructed energy. The yellow dots trace the LIGO 50% and 90% confidence contour.

peak TS values we performed a Monte Carlo study described in the next section.

2.3. Comparison with Monte Carlo simulations

To validate our interpretations of TS values we performed a detailed Monte Carlo simulation of 2 months of data (the same interval used in our analysis). The actual pointing history of the satellite was used; therefore the correct exposure of the sky was automatically taken into account. All the sources from the 3FGL catalog were kept fixed at their 3FGL catalog fluxes. As a result, the simulation is suitable

for computing the distribution of TS under the null hypothesis that no transient signal is present. With the simulated data we repeated exactly the same analysis used on real data and described in the previous section.

In Figure 5 we compare the distribution of TS_{src} obtained from flight data (filled lines) and Monte Carlo (dashed lines). We note that the Monte Carlo distributions are a good match to the distributions of the TS_{src} values obtained from the flight data, and the good absolute agreement is consistent with no statistically-significant transient counterpart being present in the flight data. Also, given the large number of trials, relatively high values of TS can be obtained in Monte Carlo simulations even if no transient signal was added. In the flight data we found 4 cases with TS>20 and with $N_\gamma > 2$, and this must be compared with the 9 cases we obtain when we analyzed the simulated data. In other words, we expected 9 false positives with $TS_{src} > 20$ (and $N_\gamma > 2$) in 2 months of flight data, and we observe 4.

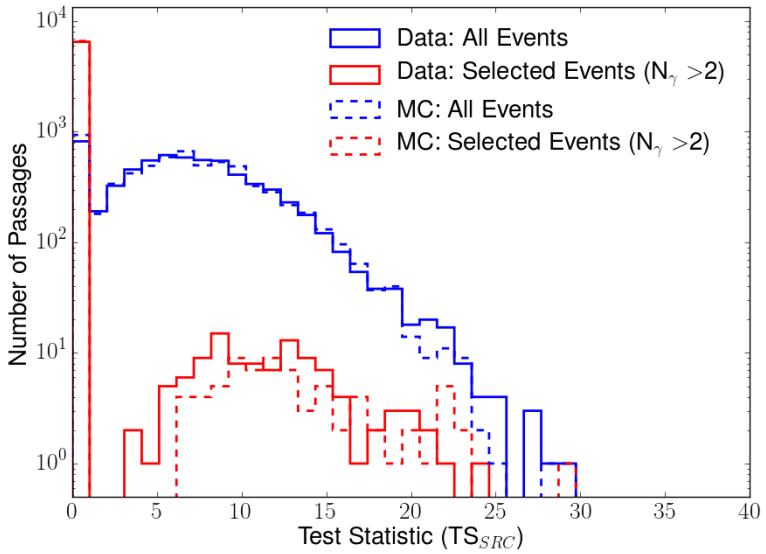


Fig. 5.— Data-Monte Carlo comparison of the distributions of the TS_{src} value. Solid lines correspond to TS distributions obtained from data, while dashed lines correspond to distributions obtained from Monte Carlo simulations. Blue lines are the distributions of the TS values when no additional selections are applied, while red corresponds to the final distribution when we require that at least three γ-rays have at least a 90% probability to be associated to the additional point source.

3. Discussion

The most promising astrophysical GW sources in the frequency range of LIGO/Virgo are the mergers of compact object binaries with NS and/or stellar-mass BH constituents. The detection of GW150914 is undoubtedly a major breakthrough in astronomy, being the first detection of GWs and the first detection of

a merging binary BH system.

Maximizing the science return from GW detections requires the identification and study of coincident EM counterparts, which would help resolve degeneracies associated with the inferred binary parameters. For example, a strong γ-ray signal may only be seen at small binary inclination relative to the sky, such that the jet (along the direction of the total angular momentum) is pointed toward us. A high-significance counterpart association would also decrease the significance threshold necessary for a confident GW detection, thereby effectively increasing the distance to which the GW signal can be detected and the searchable volume as the cube of the distance. It would help identify the host galaxy and thereby constrain or measure the merger redshift, setting the luminosity scale and allowing an independent measurement of the Hubble constant or other cosmological parameters (Metzger & Berger 2012; Cannon et al. 2012). The complementary information encoded in the EM signal (spectral and temporal evolution, energetics, inferred environment) is likewise essential to unravel the astrophysical context of the coalescence event.

The most commonly hypothesized EM counterpart of an NS-NS/NS-BH merger is a sGRB, powered by accretion onto one of the two central compact objects (Paczynski 1986; Eichler et al. 1989; Narayan et al. 1992; Rezzolla et al. 2011; Metzger & Berger 2012), which launches relativistic jets that produce a short ($<$2 s) bright flash of keV-MeV-peak γ rays followed by a broadband longer-lasting afterglow. The LAT detects approximately two sGRBs per year, with $>$100 MeV afterglows lasting up to hundreds of seconds after the trigger (Ackermann et al. 2010, 2013c), seeded by sGRB triggers from the GBM and *Swift*-BAT. The most prominent example of a LAT-detected sGRB is GRB 090510, which simultaneously triggered *Swift* and GBM, as well as causing a LAT on-board transient source trigger, resulting in a LAT localization being circulated within seconds. The LAT detected both a spike during the prompt γ-ray emission and an extended afterglow lasting hundreds of seconds, consistent with the observed optical and X-ray emission (De Pasquale et al. 2010). Figure 6 shows the $>$100 MeV γ-ray lightcurve of GRB 090510 scaled to z=0.09, the nominal redshift of GW150914 inferred from the GW observations, in comparison to the LAT upper limits described in §2.2.1. If GW150914 had had a high-energy γ-ray lightcurve similar to GRB 090510 and had been more favorably placed relative to the LAT boresight at the trigger time, it would have been easily detectable by the LAT during observations similar to those described in this paper. A GRB at the redshift of the LIGO GW source entering the field of view of *Fermi*-LAT within the first 100 s would have been detected if it were more than an order of magnitude fainter than GRB 090510.

LAT-detected long GRBs have also shown similar behavior, with a prompt spike contemporaneous with sub-MeV emission followed by long-lived emission lasting from minutes to hours with similar time dependence as radio-to-X-ray afterglows (Ackermann et al. 2013a, 2014). Although the detection rate of LAT sGRBs is low, the low redshifts of potentially detectable GW sources and therefore their potentially bright EM counterpart emission, the uncertainty in the observational signatures of GW sources, and the continuous observations of the entire sky during survey operations, make searching the LAT data for counterpart sources worthwhile.

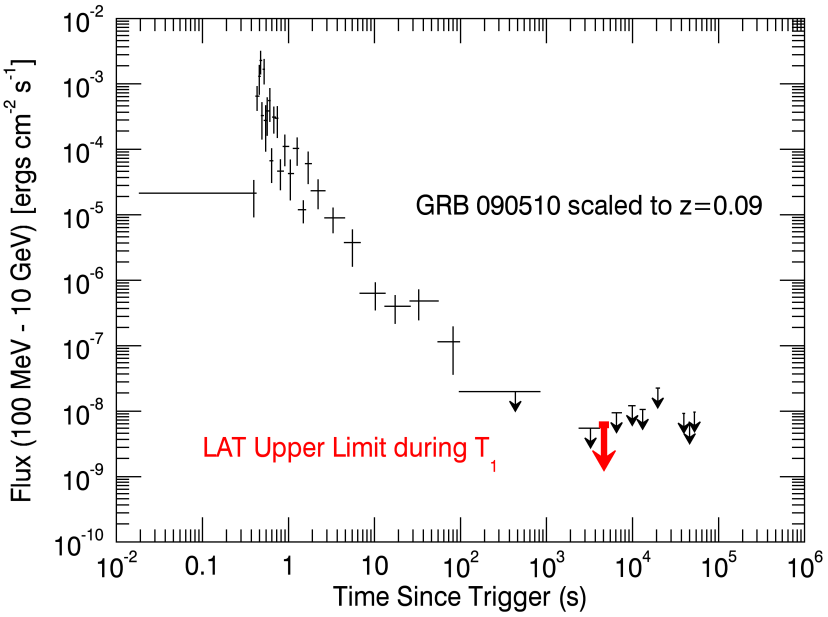


Fig. 6.— GRB 090510 is the only LAT-detected sGRB with a measured redshift (z = 0.903, Ackermann et al. 2010). We compare it here to LAT observations of GW150914. The 100 MeV–10 GeV lightcurve of GRB 090510 has been scaled to z=0.09, the redshift corresponding to the best-fit distance from the GW observation (Abbott et al. 2016). The red arrow indicates the 95% confidence upper limit measured during T_1 across the LIGO localization region and is similar to the upper limits from the measured lightcurve. Even though GRB 090510 had exceptionally bright prompt and afterglow emission, this figure demonstrates that the LAT would detect transients more than an order of magnitude fainter than GRB 090510, provided a more favorable placement of the GW candidate so that it enters the LAT FoV within 100 s of the trigger time.

3.1. LAT Searches for sGRBs

Two strategies are useful for associating EM detections of transients with GW sources. The first is to search GW data for counterparts to EM events. This was done archivally using GRB triggers for the years 2006–2011 (Aasi et al. 2014) and initial LIGO data runs, yielding no credible candidate sources (with a < 20 Mpc horizon distance). This approach is not very efficient since most of the EM events are outside the current volume sampled by the initial LIGO runs, which increases the trials factors and diminishes the GW sensitivity.

The second approach is to search for EM bursts (e.g., sGRB) related to GW events. The most promising way to find a counterpart is via a prompt trigger from the burst itself using wide FoV instruments like GBM or *Swift*-BAT. Given its large FoV and sensitivity to energies from 8 keV to 40 MeV, GBM is the most prolific detector of sGRBs currently operating, with ∼40–80 detections per year, and therefore it is very

well suited for EM counterpart searches (Connaughton et al. 2016). Yet the LAT offers several capabilities that make it a unique resource.

In the normal mode of *Fermi* GRB detection and measurement, GBM issues triggers on-board for both short and long GRBs (as well as solar flares, terrestrial γ-ray flashes, magnetar flares, and other short, hard X-ray/soft γ-ray transients), and approximately half of the GBM GRBs occur in the LAT FoV. However, in cases of high peak brightness, GBM initiates an automated repoint of the *Fermi* spacecraft to optimize LAT observations over the next 2.5 hours. Regardless of whether an automated pointing is triggered, even during normal sky survey operations, the LAT will observe the entire sky within 2 orbits ($\sim$ 3 hours), fully covering 100% of any GW localization contour, making follow-up observations of GW triggers both automatic and routine. Neither instrument on *Fermi* has observing constraints limiting the viewing near the Sun or Moon.

If the LAT were to detect a counterpart to a GW trigger, it has the distinct advantage of providing smaller localization uncertainties than GBM. Typical GBM localizations have radii of several degrees plus systematic uncertainties of 3–14° (Connaughton et al. 2015), while LAT localizations have radii $\sim 0.1-1^\circ$. A LAT detection would substantially reduce the sky area for follow-up observations at other wavelengths, some of which require extensive tiling campaigns over days after a trigger to cover a significant fraction of the GW localization region (Evans et al. 2016; LIGO Collaboration et al. 2016). Although the LAT obtained an on-board localization for short GRB 090510 (Ackermann et al. 2010) within 15 seconds, LAT localizations typically have an $\sim$8-hr latency for data transmission and ground processing.

The LAT has also recently (as of 2015 June) benefited from a major upgrade to the event reconstruction analysis pipeline, known as Pass 8 (Atwood et al. 2013). Pass 8 improves the LAT sensitivity due to increased photon acceptance, especially at low ($<$100 MeV) and high energies ($>$10 GeV), and reduces localization radii by $\sim$ 30%. Combined with new analysis pipelines that search for transients on all timescales (Vianello et al. 2015), the LAT is now better suited to discover counterparts to GW sources in both automated pipelines and the specialized searches described in §2.

The LIGO EM follow-up partners conducted large follow-up campaigns in the optical, radio, and X-ray to search for a counterpart to GW150914 (LIGO Collaboration et al. 2016). Similar campaigns will occur for other GW triggers no matter the likely progenitor and regardless of whether it is observed along the putative jet axis. Although no orphan GRB afterglows (which are expected to be associated with off-axis observing angles) have conclusively been detected, models (Granot et al. 2002; van Eerten et al. 2010) predict delayed, fainter transient emission from the afterglow itself, an isotropic optical-near-infrared kilonova signature (Li & Paczyński 1998). Other potential EM counterparts have been theorized, including late radio emission from mildly relativistic material that is dynamically ejected during the merger and drives a shock into the external medium (Nakar & Piran 2011), and radio-to-X-ray (or γ-ray) emission over seconds to days from relativistic ejecta created as the NSs collide during their merger (Kyutoku et al. 2014). Given the capability of the LAT to detect transients on timescales from milliseconds to years, careful searches for possible afterglow emission within the LIGO localization area over relevant timescales after the GW trigger are essential and require no change to the *Fermi* observing strategy.

High-energy γ-ray emission from GRBs observed by the LAT above 100 MeV lasts much longer (min-

utes to hours) than the prompt emission observed by the GBM (Ackermann et al. 2013c), for both long and short GRBs (Abdo et al. 2010; De Pasquale et al. 2010). Therefore, even if a localization probability region from LIGO/Virgo is outside the FoV of the LAT during the time of the trigger, the instrument could detect temporally-extended emission in the minutes following the prompt signal, when the region re-enters its FoV. This could result in a much more precise localization of the EM counterpart.

3.2. EM Counterparts to BH Binary Mergers

As discussed in Abbott et al. (2016), the GW150914 waveform is consistent with the expectation for the merger of two stellar-mass BHs. The comparatively clean waveform in the "chirp" phase before the merger and the "ring-down" stage after the merger would not naturally be expected from coalescing NSs, which possess matter distributed outside an event horizon. The expected progenitors of sGRBs are NS-NS or NS-BH binaries (Giacomazzo et al. 2013; Paczynski 1986; Eichler et al. 1989; Narayan et al. 1992; Rezzolla et al. 2011; Metzger & Berger 2012). Therefore, a classical sGRB counterpart to GW150914 is not expected.

Prior to the discovery of GW150914, studies focusing on EM counterparts to stellar-mass BH mergers were few in number. Most of the numerical simulations have focused on supermassive BH mergers, where circumbinary disk formation is expected with ample gas supply available to power an EM counterpart (Mayer et al. 2007). Stellar-mass BH mergers should require a substantial quantity of nearby gas to form the disk-jet system that is expected to be necessary for an EM counterpart to be detectable at tens-to-hundreds of Mpc distances. The weak counterpart candidate detected by the GBM described by Connaughton et al. (2016) poses an interesting dilemma for theoretical models, if it is connected to GW150914. Unfortunately, since the GW localization region was not in the FoV of the LAT at the time of the GW trigger, the prompt signal from the GBM candidate could not be addressed with the LAT observations. Should such γ-ray associations arise for future LIGO events, a new paradigm for these mergers will be indicated.

4. Conclusions

The *Fermi*-LAT is uniquely capable of searching for high-energy γ-ray counterparts to sources detected by GW observatories. We use this capability to undertake a detailed search in the regular LAT survey data for a counterpart temporally and spatially coincident with the LIGO trigger on GW150914. Although GW150914 was not in the LAT FoV at the trigger time, the LAT observed the entire region within ~ 70 minutes of the GW trigger. We searched on short and long timescales for evidence of a transient γ-ray source contemporaneous with GW150914. No LAT counterpart is detected, and upper limits have been set on the GeV γ-ray flux within the LIGO localization.

As the sensitivity of LIGO and Virgo improve over the next few years, their detection horizon for NS-NS and NS-BH binary mergers, and thus the likelihood of sGRB coincidence, will increase greatly. The merger rates are highly uncertain and depend on the populations and evolution of binaries and opening

angles of sGRB jets. The coincident detection of prompt γ-ray signals, with on-axis or potentially off-axis afterglow signals will teach us about the physics of binary mergers. With the discovery of GW150914, the search for EM-GW coincidences enters a new phase. It is important to test the strong expectation that stellar BH mergers do not radiate much light; it is equally important to refine the techniques that will be needed to associate sGRBs with GW events from NS mergers. The approach described in this communication is well suited to achieve these twin goals when LIGO detects more GW events.

The *Fermi* LAT Collaboration acknowledges generous ongoing support from a number of agencies and institutes that have supported both the development and the operation of the LAT as well as scientific data analysis. These include the National Aeronautics and Space Administration and the Department of Energy in the United States, the Commissariat à l'Energie Atomique and the Centre National de la Recherche Scientifique / Institut National de Physique Nucléaire et de Physique des Particules in France, the Agenzia Spaziale Italiana and the Istituto Nazionale di Fisica Nucleare in Italy, the Ministry of Education, Culture, Sports, Science and Technology (MEXT), High Energy Accelerator Research Organization (KEK) and Japan Aerospace Exploration Agency (JAXA) in Japan, and the K. A. Wallenberg Foundation, the Swedish Research Council and the Swedish National Space Board in Sweden. Additional support for science analysis during the operations phase is gratefully acknowledged from the Istituto Nazionale di Astrofisica in Italy and the Centre National d'Études Spatiales in France.

REFERENCES

Abramovici, A., Althouse, W. E., Drever, R. W. P., et al. 1992, Science, 256, 325

Aasi, J., Abbott, B. P., Abbott, R., et al. 2014, Phys. Rev. D, 89, 122004

Abbott, B. P., Abbott, R., Abbott, T. D., et al. 2016, Phys. Rev. Lett., 116, 061102

Abbott, B. P., Abbott, R., Adhikari, R., et al. 2009, Phys. Rev. D, 80, 102001

Abbott, B. P., Abbott, R., Abbott, T. D., et al. 2016, The Astrophysical Journal Letters, 818, L22

Abdo, A. A., Ackermann, M., Ajello, M., et al. 2010, ApJ, 712, 558

Acernese, F., Alshourbagy, M., Antonucci, F., et al. 2009, Classical and Quantum Gravity, 26, 085009

Acero, F., Ackermann, M., Ajello, M., et al. 2015, ApJS, 218, 23

Ackermann, M., Asano, K., Atwood, W. B., et al. 2010, ApJ, 716, 1178

Ackermann, M., Ajello, M., Asano, K., et al. 2013a, ApJ, 763, 71

Ackermann, M., Ajello, M., Albert, A., et al. 2013b, ApJ, 771, 57

Ackermann, M., Ajello, M., Asano, K., et al. 2013c, ApJS, 209, 11

—. 2014, Science, 343, 42

Atwood, W., Albert, A., Baldini, L., et al. 2013, ArXiv e-prints, arXiv:1303.3514 [astro-ph.IM]

Atwood, W. B., Abdo, A. A., Ackermann, M., et al. 2009, ApJ, 697, 1071

Cannon, K., Cariou, R., Chapman, A., et al. 2012, ApJ, 748, 136

Caron, B., Derome, L., Flaminio, R., et al. 1999, Astroparticle Physics, 10, 369

Chiang, J. 2012, Automated Science Processing for the Fermi Large Area Telescope, ed. M. J. Way, J. D. Scargle, K. M. Ali, & A. N. Srivastava, 41

Ciprini, S., Thompson, D. J., & on behalf of the Fermi LAT collaboration. 2013, ArXiv e-prints, arXiv:1303.4054 [astro-ph.HE]

Connaughton, V., G., et al. 2016, in-prep

Connaughton, V., Briggs, M. S., Goldstein, A., et al. 2015, ApJS, 216, 32

De Pasquale, M., Schady, P., Kuin, N. P. M., et al. 2010, ApJ, 709, L146

Eichler, D., Livio, M., Piran, T., & Schramm, D. N. 1989, Nature, 340, 126

Evans, P. A., Osborne, J. P., Kennea, J. A., et al. 2016, MNRAS, 455, 1522

Giacomazzo, B., Perna, R., Rezzolla, L., Troja, E., & Lazzati, D. 2013, ApJ, 762, L18

Górski, K. M., Hivon, E., Banday, A. J., et al. 2005, ApJ, 622, 759

Granot, J., Panaitescu, A., Kumar, P., & Woosley, S. E. 2002, ApJ, 570, L61

Kocevski, D., Ajello, M., Buehler, R., Becerra, J., & Ojha, R. 2014, The Astronomer's Telegram, 6098

Kyutoku, K., Ioka, K., & Shibata, M. 2014, MNRAS, 437, L6

Li, L.-X., & Paczyński, B. 1998, ApJ, 507, L59

LIGO Collaboration, V., et al. 2016, in-prep

Mattox, J. R., et al. 1996, ApJ, 461, 396

Mayer, L., Kazantzidis, S., Madau, P., et al. 2007, Science, 316, 1874

Meegan, C., Lichti, G., Bhat, P. N., et al. 2009, ApJ, 702, 791

Metzger, B. D., & Berger, E. 2012, ApJ, 746, 48

Nakar, E., & Piran, T. 2011, Nature, 478, 82

Narayan, R., Paczynski, B., & Piran, T. 1992, ApJ, 395, L83

Omodei, N., et al. 2015, Gamma-ray Coordinates Network Circular #18709

Paczynski, B. 1986, ApJ, 308, L43

Protassov, R., van Dyk, D. A., Connors, A., Kashyap, V. L., & Siemiginowska, A. 2002, ApJ, 571, 545

Rezzolla, L., Giacomazzo, B., Baiotti, L., et al. 2011, ApJ, 732, L6

Sathyaprakash, B. S., & Schutz, B. F. 2009, Living Reviews in Relativity, 12, arXiv:0903.0338 [gr-qc]

van Eerten, H., Zhang, W., & MacFadyen, A. 2010, ApJ, 722, 235

Vianello, G., Omodei, N., & Fermi LAT collaboration. 2016, in American Astronomical Society Meeting Abstracts, Vol. 227, American Astronomical Society Meeting Abstracts, #416.01

Vianello, G., Omodei, N., & Fermi/LAT collaboration. 2015, ArXiv e-prints, arXiv:1502.03122 [astro-ph.HE]

Wilks, S. S. 1938, Ann. Math. Stat., 9, 60

A. *Fermi*-LAT likelihood analysis

The standard tools for *Fermi*-LAT analysis, the *Fermi* `ScienceTools`, are available for download from the FSSC[8], where the LAT data can also be downloaded. In all analyses presented in this paper we used the Pass 8 data class `P8R2_TRANSIENT010E_V6`, and the ST v10r0p5. The `ScienceTools` are based on the standard maximum likelihood analysis: a model summarizing knowledge about the sources of γ rays in a particular region of the sky is convolved with the instrument response and optimized over its parameters to maximize the likelihood that the model best represents the data. The details on how to perform such an analysis with LAT data are described on the FSSC website; here we summarize the main steps. We start by selecting all the data within a given energy range and contained within a ROI. In the case of the *unbinned likelihood* analysis used in this paper, the ROI is circular and is therefore characterized by a center and a radius. Since the upper layers of the Earth's atmosphere are a bright source of γ rays that are very difficult to model in the likelihood analysis, we need to further reduce the Earth Limb contamination in the data. At the altitude of the nearly-circular *Fermi* orbit, the limb is always seen by the LAT at an angle of $\sim 113^\circ$ from the zenith direction. We therefore remove all photons with zenith angles larger than a threshold that depends on the minimum energy used in the analysis (since the PSF is larger at lower energies). In this paper we define the size of the ROI, the energy range and the zenith angle limit used in each analysis in the

This preprint was prepared with the AAS LaTeX macros v5.2.

[8] `http://fermi.gsfc.nasa.gov/ssc/data/analysis/`

respective sections.

A.1. Source significance

The significance of a new source S in a likelihood analysis is determined by using the Likelihood Ratio Test (LRT). The TS of S is equal to twice the logarithm of the ratio of the maximum likelihood value produced with a model including S to the maximum likelihood value of the null hypothesis, i.e., a model that does not include S. The reference distribution for TS can be used to determine the probability that a measured TS for a source is due to a statistical fluctuation of the null hypothesis (p-value). Unfortunately, the probability density function in a source-over-background test like this cannot, in general, be described by an asymptotic distribution such as expected from Wilks' theorem (Wilks 1938; Protassov et al. 2002). However, it has been verified by dedicated Monte Carlo simulations (Mattox et al. 1996) that the distribution of TS under the null hypothesis is approximately equal to a $\chi^2_{n_{dof}}/2$ distribution[9], where n_{dof} is the number of degrees of freedom associated with the new source. In all cases considered in this paper the new source has a fixed position and a power-law spectrum with two parameters, hence $n_{dof} = 2$. However, in this paper we search on a large region of the sky and over different timescales, and thus we must also account for the trials factor, as explained in the next section.

A.2. TS maps and trial factors

Test Statistic maps (TS maps) are used to probe for a source at an unknown location and are obtained by moving a test source by regular steps over a grid and re-optimizing the model parameters to maximize the likelihood. The size of the steps is usually a fraction of the size of the PSF. Since the PSF depends on the energy, we consider the size of the PSF at the minimum energy considered for the map. In our case, we chose a step of $0.^\circ2$. The maximum (denoted TS_{max}) of the map corresponds to the most likely localization for a new source. A likelihood analysis with an ROI centered on the position of TS_{max} gives then the final value TS_{src} for the candidate source. However, the search over the grid involves a certain number of non-independent trials, hence the reference distribution of TS_{src} is unknown and must be determined case-by-case with Monte Carlo simulations, as in this work.

B. TS maps for the long-baseline search

For the TS maps of the long-baseline search we use the largest grid fitting inside each of the 9 ROIs. We model the background by taking into account the isotropic component (defined in the template file

[9]The factor of ½ in front of the TS PDF formula results from allowing only positive source fluxes.

`iso_P8R2_TRANSIENT010E_V6_v06.txt`), which includes the extragalactic diffuse γ radiation and residual charged-particle contamination, and the Galactic diffuse γ-ray emission (using the spatial and spectral template in `gll_iem_v06.fits`), which is the result of interaction of cosmic rays with the gas and the electromagnetic field of the Milky Way. The normalization of the first is left free to vary in order to accommodate orbital variations, while the Galactic diffuse emission model is held fixed to its nominal value. All the point sources from the 3FGL catalog (Acero et al. 2015) are also included with their parameters fixed.

In Figure 7 we display the TS maps for each region integrated from t_{GW} to t_{GW}+10 ks. The 3FGL sources have been overlaid as yellow stars while the white circles represent the *Fermi*-LAT γ rays (the size of the circle is proportional to the reconstructed energy of the event).

C. *Fermi*-LAT point sources

For completeness, we report the *Fermi*-LAT sources in the 3FGL catalog that are present in each ROI, with, where available, source and class associations. Since the integration times in our analysis are much shorter than the integration time of the catalog, we select only those sources with an average significance (`Signif_Avg` in the 3FGL) >20, which roughly corresponds to an average flux in the range 10^{-9}–10^{-7} ph cm^{-2} s^{-1} in the energy range 0.1–1 GeV.

Table 1. ROIs and the 3FGL sources they contain

ROI (R.A.,Dec.)	R.A. deg	Dec. deg	3FGL Name	Association	Class[a]
ROI_0 (150.0, −6.4)	147.223	0.363	3FGL J0948.8+0021	PMN J0948+0022	NLSY1
	148.255	−8.663	3FGL J0953.0-0839	PMN J0953-0840	bll
ROI_1 (153.0, −48.0)	155.790	−57.759	3FGL J1023.1-5745	LAT PSR J1023-5746	PSR
	159.735	−53.186	3FGL J1038.9-5311	MRC 1036-529	bcu
	164.499	−52.455	3FGL J1057.9-5227	PSR J1057-5226	PSR
ROI_2 (146.0, −63.0)	136.218	−57.570	3FGL J0904.8-5734	PKS 0903-57	bcu
	143.481	−62.534	3FGL J0933.9-6232		
	154.730	−58.946	3FGL J1018.9-5856	1FGL J1018.6-5856	HMB
	155.790	−57.759	3FGL J1023.1-5745	LAT PSR J1023-5746	PSR
	157.123	−58.320	3FGL J1028.4-5819	PSR J1028-5819	PSR
	158.926	−67.334	3FGL J1035.7-6720		
	161.129	−57.630	3FGL J1044.5-5737	LAT PSR J1044-5737	PSR
	161.277	−59.692	3FGL J1045.1-5941	Eta Carinae	BIN
	162.067	−58.535	3FGL J1048.2-5832	PSR J1048-5832	PSR
ROI_3 (131.0, −68.0)	122.811	−75.492	3FGL J0811.2-7529	PMN J0810-7530	bll
	143.481	−62.534	3FGL J0933.9-6232		
ROI_4 (115.0, −70.0)	90.313	−70.609	3FGL J0601.2-7036	PKS 0601-70	fsrq
	98.942	−75.293	3FGL J0635.7-7517	PKS 0637-75	fsrq
	101.088	−67.223	3FGL J0644.3-6713	PKS 0644-671	bcu
	105.158	−66.173	3FGL J0700.6-6610	PKS 0700-661	bll
	122.811	−75.492	3FGL J0811.2-7529	PMN J0810-7530	bll
ROI_5 (98.0, −71.0)	81.650	−68.420	3FGL J0526.6-6825e	LMC	GAL
	90.313	−70.609	3FGL J0601.2-7036	PKS 0601-70	fsrq
	98.942	−75.293	3FGL J0635.7-7517	PKS 0637-75	fsrq
	101.088	−67.223	3FGL J0644.3-6713	PKS 0644-671	bcu
	105.158	−66.173	3FGL J0700.6-6610	PKS 0700-661	bll
	122.811	−75.492	3FGL J0811.2-7529	PMN J0810-7530	bll
ROI_6 (80.0, −71.0)	79.189	−62.121	3FGL J0516.7-6207	PKS 0516-621	bll
	81.650	−68.420	3FGL J0526.6-6825e	LMC	GAL
	90.313	−70.609	3FGL J0601.2-7036	PKS 0601-70	fsrq
	98.942	−75.293	3FGL J0635.7-7517	PKS 0637-75	fsrq
	101.088	−67.223	3FGL J0644.3-6713	PKS 0644-671	bcu

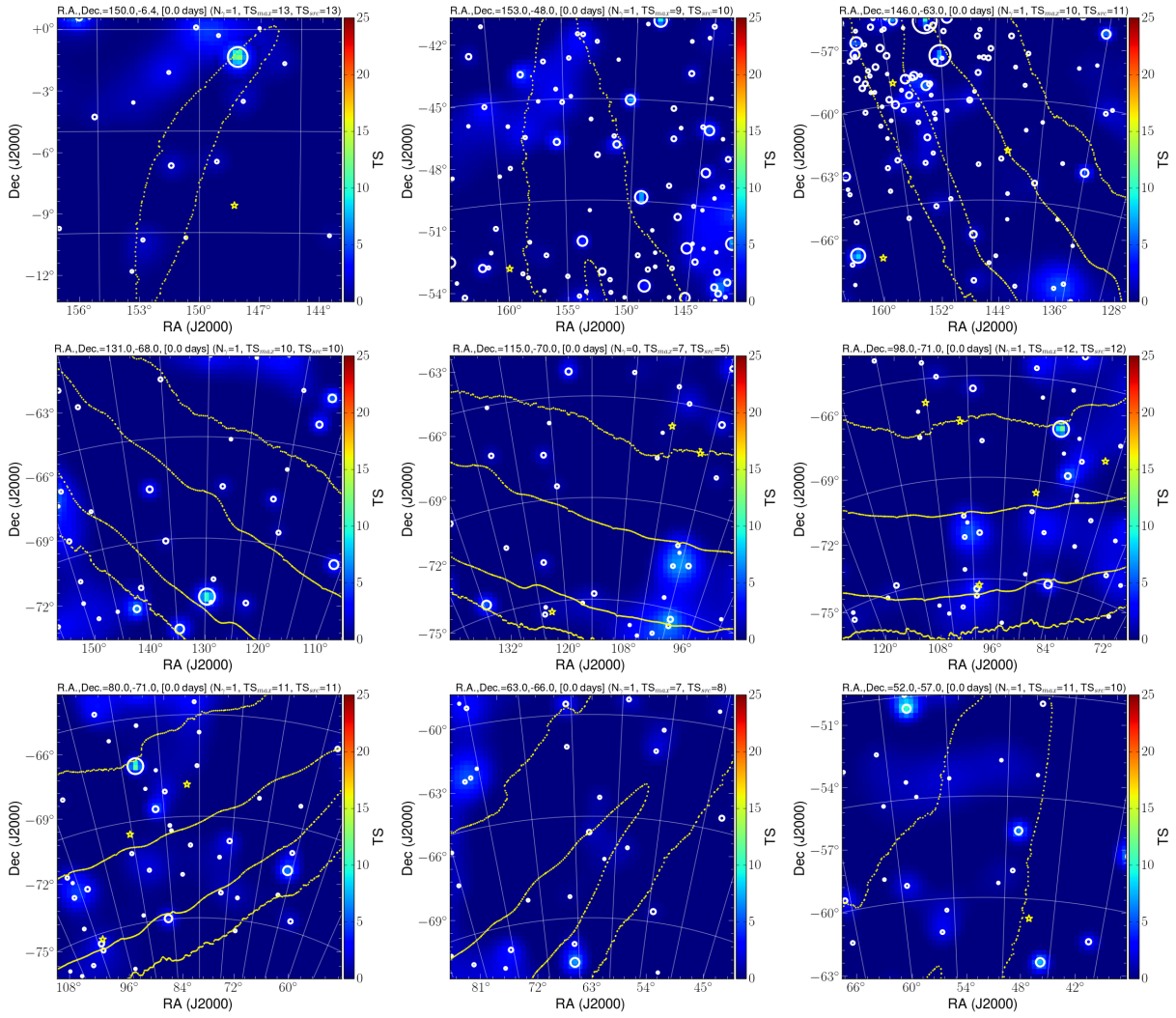


Fig. 7.— TS maps for the nine ROIs used in our analysis integrated from t_{GW} to t_{GW}+10 ks. Stars indicate the 3FGL sources in each field, the white circles are the individual LAT γ rays (with the size proportional to their reconstructed energy). The yellow dots trace the LIGO 90% contour.

Table 1—Continued

ROI (R.A.,Dec.)	R.A. deg	Dec. deg	3FGL Name	Association	Class[a]
ROI_7 (63.0, −66.0)	47.478	−60.963	3FGL J0309.9-6057	PKS 0308-611	fsrq
	76.780	−61.050	3FGL J0507.1-6102	PKS 0506-61	fsrq
	79.189	−62.121	3FGL J0516.7-6207	PKS 0516-621	bll
	81.650	−68.420	3FGL J0526.6-6825e	LMC	GAL
ROI_8 (52.0, −57.0)	39.195	−61.600	3FGL J0236.7-6136	PKS 0235-618	fsrq
	47.478	−60.963	3FGL J0309.9-6057	PKS 0308-611	fsrq

[a]Class names are from the 3 FGL catalog (Acero et al. 2015).